Journal of Power Sources 222 (2013) 390–399

Contents lists available at SciVerse ScienceDirect

Journal of Power Sources

journal homepage: www.elsevier.com/locate/jpowsour

Investigation of Pd-based electrocatalysts for oxygen reduction in PEMFCs operating under automotive conditions

A. Stassi, I. Gatto, V. Baglio, E. Passalacqua, A.S. Aricò*

CNR-ITAE Istituto di Tecnologie Avanzate per l'Energia "Nicola Giordano", Via Salita S. Lucia sopra Contesse 5, 98126 Messina, Italy

HIGHLIGHTS

- Pd-based electrocatalysts are prepared by using a sulphite-complex route.
- Structure, morphology and surface characteristics are investigated.
- Better surface characteristics are recorded with the two-step Pd catalyst.
- Pd-based catalyst shows a significant increase of performance at 110 °C.
- Pd-based composite catalysts get advantage of operation under automotive conditions.

GRAPHICAL ABSTRACT

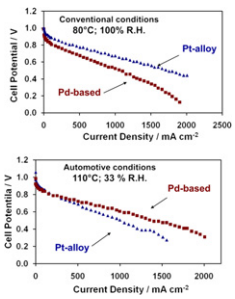

ARTICLE INFO

Article history:
Received 13 June 2012
Received in revised form
5 August 2012
Accepted 2 September 2012
Available online 10 September 2012

Keywords:
Pd catalysts
Oxygen reduction reaction
Polymer electrolyte membrane fuel cells
Intermediate temperature
Automotive

ABSTRACT

Composite Pd-based electrocatalysts consisting of a surface layer of Pt (5% wt.) supported on a core Pd_3Co_1 alloy were prepared. Two preparation approaches were investigated. One consisting of a single-step reduction procedure; in the second method, preparation of the PdCo alloy and deposition of a Pt overlayer occurred in two distinct steps. The catalyst prepared by a one-step process showed oxidised Pt species on the surface even if characterized by a smaller crystallite size with respect to the two-step Pd-based catalyst (4 nm vs. 6 nm). Moreover, the two-step process showed an enrichment of Pt on the surface and a smaller content of Co in the outermost layers. The enhanced surface characteristics of the two-step Pd catalyst resulted in a better performance. At 80 °C, the mass activity was lower than a Pt_3Co_1 alloy catalyst with the same crystallographic structure. Interestingly, the composite PtPdCo catalyst showed a significant increase of performance as the temperature was increased to 110 °C whereas the Pt_3Co_1 showed a decrease due to a prevailing effect of ionomer dry-out in the catalytic layer. The composite catalyst appeared sufficiently stable after 10^4 electrochemical cycles between 0.6 and 0.9 V at 110 °C and 33% R.H.

1. Introduction

Highly dispersed carbon-supported nanosized Pt particles are presently the benchmark electrocatalyst for polymer electrolyte fuel cells (PEMFCs) [1–7]. The rate determining step is the oxygen reduction reaction which occurs at large cathodic overpotentials, e.g. overpotentials greater than 0.4 V for current densities of practical interest, e.g. 1 A cm^{-2} and with Pt loadings as high as 0.4 mg cm^{-2} [2,7]. Large efforts have been made in the last decades to significantly reduce the Pt loading while maintaining suitable performance essentially by increasing Pt utilization. Novel approaches to form nanostructured materials or thin film nanostructured catalyst layers with an extension of the triple phase boundary have provided promising results [8–11]. At the same time, the development of

* Corresponding author. Tel.: +39 090624237; fax: +39 090624247.
E-mail addresses: arico@itae.cnr.it, antonino.arico@itae.cnr.it (A.S. Aricò).

0378-7753/$ – see front matter © 2012 Elsevier B.V. All rights reserved.
http://dx.doi.org/10.1016/j.jpowsour.2012.09.002

suitable binary and ternary Pt-alloys, e.g. PtCo, PtNi, PtCoCr, PtCoMn has allowed to increase considerably the mass activity with respect to the conventional Pt/C providing a basis for Pt content reduction [2,6,9–13]. Yet, the continuous increase of the cost of Pt has made less effective such progresses. Moreover, an increase in mass activity using Pt-alloys or nanostructured catalysts, as observed under rotating disc configuration, often does not correspond to a proportional increase of power density in fuel cells at practical cell voltages, e.g. 0.65 V, of interest for automotive applications. This is because the contribution of other effects such as ohmic constraints and mass transfer polarizations becomes more relevant as the fuel cell current density increases. As alternative to Pt, pyrolized cobalt or iron porphyrins [14,15], non-precious metals/heteroatomic polymers [16], transition metal chalcogenides [17] have been actively investigated. Although the recently achieved performances appear very promising, the main drawbacks regard a poor stability during fuel cell operation at relevant current densities and a low voltage efficiency. In the transition process from Pt to cheaper non Pt-group (NPG) metals or non-precious catalysts, Pd-based electrocatalysts appear as a proper compromise. Pd shows a suitable electrocatalytic activity for the oxygen reduction reaction, even though lower than Pt, whereas its cost is at present significantly lower than Pt and its reserves much wider [18]. Several attempts have been made to develop Pt–Pd catalysts especially with the aim to take advantage of a possible synergistic effect; however, the ORR activity for Pd-based electrocatalysts is generally lower than that of Pt-rich electrocatalysts [19–23]. However, stable and highly performing Pt-alloys are characterized by large excess of Pt content (e.g. formulations such as Pt_3Co_1), thus providing limited perspectives to reduce consistently the Pt content. On the other hand Pt-alloys, such as PtCu, with large non-noble metal content give rise to significant dealloying during practical operation. This may cause performance degradation due to the poisoning of membrane sulphonic groups as a consequence of an ion-exchange process between protons and the dissolved transition metal ions. A controlled electrochemical dealloying approach during the fuel cell conditioning process and subsequent purification in acid solutions of the MEA containing the de-alloyed catalyst has been suggested [6]. Although this approach is interesting to increase the mass activity, it appears not easily applicable to stack manufacturing.

Pd-based electrodes may represent a consistent way to reduce the Pt content in PEMFCs [18] and provide a performance that is not significantly lower than Pt/C [24,25]. One interesting approach to reduce the Pt loading while maintaining proper activity and stability is to form a Pt monolayer on Pd or Pd-alloys [26–28]. In the case of a Pt monolayer coated on annealed-Pd_3Fe single crystals, two positive effects were observed: (i) a downshift of the Pd d-band center relative to pure Pd caused by the alloying with Fe, and (ii) a suitable interaction between the segregated Pt layer and Pd. In particular, the first effect caused a decreased interaction of oxygen species (e.g. OH) with Pd favouring oxygen molecules adsorption and dissociation [26–28].

Various procedures have been used for preparing Pt and Pd fuel cell catalysts. These include polyol or borohydride reduction, microemulsion method, formic acid reduction of Pt and Pd precursors, electroless deposition of Pt on Pd, etc.[18,24,25,29–39]. One of the main drawback is the increase of particle size passing from Pt-rich to Pd-rich catalysts. Nanodendrites and core-shell type Pd electrocatalysts appear useful to increase the ORR activity [29,40,41].

The approach pursued in this work is based on the synthesis of an inorganic salt of Pd (Pd–sulphite complex) which is then decomposed on the surface of a carbon black support in solution forming colloidal amorphous nanoparticles which are easily impregnated by a Co precursor. After a thermal treatment, PdCo nanoparticles surface-enriched in Pd are obtained. These are successively covered by a Pt layer using a colloidal solution obtained from a similar Pt–sulphite complex.

A commonly used technique to investigate Pt nanoparticles engineering, in particular the occurrence of a surface segregation of Pt (Pt skin layer, Pt skeleton layer, percolated and core-shell structures, etc. [6,12,13]), is based on the use of aberration-corrected high-angle annular dark-field in the scanning transmission electron microscope in combination with energy dispersion spectroscopy [13]. This technique while providing useful information on a local basis appears more accurate for nanoparticles of dimensions in the range of 10 nm. Moreover, it provides an information concerning with a few selected nanoparticles that may not be a representative of the overall sample. The approach used in this work involves low-energy ion scattering spectroscopy (LE-ISS) using $3He^+$ ions at low accelerating voltage (1 kV). The kinetic energy of the reflected $3He^+$ is analysed to get information on the chemistry of the outermost layer. Depth profiling in this work is carried out by combining LE-ISS with X-ray photoelectron spectroscopy (XPS) and X-ray fluorescence (XRF).

Another aspect concerns with the effect of temperature. Most of the recently investigated Pd-based catalysts have been studied in rotating disc configuration at room temperature or under PEMFC at the conventional temperature of 80 °C. Whereas, for automotive applications, operation at intermediate temperatures such as 110–130 °C can mitigate the constraints concerning with thermal and water management simplifying the fuel cell system, reducing its volume inside the car with a strong impact on costs and reliability [42]. The pre-requisites of an electrolyte for automotive applications are a good capability of operation in the intermediate temperature range as well as at conventional and low temperatures as required by a rapid or cold start-up. Recent progresses include short side chain perfluorosulfonic electrolyte membranes, composite membranes and novel electrolyte polymers [42–45]. However, since the aim of this study is concerned with the assessment of the Pd-based catalysts at both conventional and intermediate temperatures, we have preferred to work with conventional Nafion membranes under pressurised mode thus avoiding complete membrane dehydration above 100 °C [7].

In order to assess the performance of Pd-rich catalysts with respect to benchmark Pt-based catalysts, a comparison with a Pt_3Co_1/C catalyst characterised by the same crystallographic structure which has been shown previously to perform better than Pt/C [42] is made.

2. Experimental

2.1. Catalyst preparation

Cathodic Pd-based catalysts consisted of 5% wt. Pt and 95% wt. Pd–Co. The nominal core alloy atomic composition was Pd_3Co_1. The total metal fraction on carbon was 50% wt. Ketjenblack EC (KB) carbon black with BET surface area of 850 $m^2 g^{-1}$ was used as conductive support.

Two preparation procedures were used for the Pd-based catalysts. In both procedures $Na_6Pt(SO_3)_4$ and $Na_6Pd(SO_3)_4$ salts were prepared by reaction of H_2PtCl_6 and $PdCl_4$ with sodium dithionite. The Pd–sulphite salt was first dissolved in acidic solution and subsequently decomposed with H_2O_2 to form a colloidal dispersion that was impregnated on the carbon black. Co was deposited by incipient wetness of cobalt nitrate on the amorphous PdOx/C catalyst previously obtained. The concentration of $Co(NO_3)_2$ was adjusted to achieve a Pd/Co atomic ratio of 3:1 in the final catalyst. The obtained amorphous catalyst was thus thermal treated in Ar atmosphere at 500 °C to form PdCo alloy nanoparticles (carbothermal reduction). To achieve a Pd surface enrichment, the treated

sample was pre-leached at 80 °C in 0.5 M $HClO_4$. The sample was subsequently impregnated with a colloidal solution of Pt obtained by decomposition of $Na_6Pt(SO_3)_4$ with H_2O_2. The Pt overlayer was reduced in a mixture of H_2/Ar. The described procedure is reported through the text as two-step process. A variation to this process consisted of the impregnation of the untreated amorphous PdCoOx/C with a colloidal solution of Pt obtained by decomposition of $Na_6Pt(SO_3)_4$ with H_2O_2 followed by reduction in a mixture of H_2/Ar. This latter is reported in the text as one-step process since only one reduction process is used.

For comparison, a Pt_3Co_1/KB catalyst prepared by a similar sulphite complex route and carbothermal reduction [42] having the same face centered cubic (fcc) crystallographic structure of the Pd-based catalysts was tested under same conditions.

A 30% Pt/Vulcan XC-72R catalyst obtained by a similar procedure was used at the anode.

2.2. Physico-chemical analysis

The catalysts were characterised by X-ray diffraction (XRD) using a Philips X-pert 3710 X-ray diffractometer with Cu K*a* radiation operating. The peak profile of the (220) reflection in the face centered cubic structure of Pt-alloy and composite Pd-based catalysts was analysed using the Marquardt algorithm and it was used to calculate the crystallite size by the Debye–Scherrer equation [42]. Instrumental broadening was determined by using a standard Pt sample. X-ray fluorescence analysis of the catalysts was carried out by a Bruker AXS S4 Explorer spectrometer. The total metal content in the catalysts was determined by burning the carbon support in a thermal gravimetry experiment at 950 °C in air. Transmission electron microscopy (TEM) analysis was made by first dispersing the catalyst powder in isopropyl alcohol. A few drops of these solutions were deposited on carbon film-coated Cu grids and analysed with a FEI CM12 microscope.

X-ray photoelectron spectroscopy (XPS) measurements were performed by using a Physical Electronics (PHI) 5800-01 spectrometer. A monochromatic Al Kα X-ray source was used at a power of 350 W. XPS data have been interpreted by using the on-line library of oxidation states implemented in the PHI MULTIPAK 6.1 software and the PHI Handbook of X-ray photoelectron spectroscopy [46].

For LE-ISS measurements, the polarity of the analyzer in the PHI 5800-01 spectrometer was switched from XPS to ISS mode, a 3He-feed ion gun operating at low voltage (1 kV) was used [42].

2.3. Electrochemical studies

The electrodes were prepared according to the procedure described in a previous report [7]; they consisted of carbon cloth backings, diffusion and catalytic layers. The catalytic layer was composed of 33 wt.% Nafion ionomer (1100 g/eq.) and 67 wt.% catalyst. For the Pd-based cathodes in all experiments, excluding the accelerated degradation test, the Pt loading was 0.015 mg cm^{-2} and Pd loading was 0.24 mg cm^{-2}. In the accelerated degradation test, the Pt loading for the Pd-based cathodes was 0.012 mg cm^{-2}, Pd loading was 0.19 mg cm^{-2}. In all tests involving the Pt_3Co_1 alloy catalyst, the Pt loading was 0.3 mg cm^{-2}. MEAs were formed by a hot-pressing procedure and subsequently installed in a fuel cell test fixture. A Nafion 115 membrane (~120 μm) was preferred to thinner PFSA membranes in order to reduce the effect of H_2 cross-over which may affect the in-situ determination of the mass activity at 0.9 V RHE. In the various MEAs, the anode was maintained constant (Pt/C, 0.3 mg cm^{-2}) whereas the cathode was varied by using the catalysts described above.

The cell test fixture was connected to a fuel cell test station. An AUTOLAB Metrohm potentiostat/galvanostat equipped with a 20 A current booster was used for electrochemical diagnostics. The humidifier temperature was varied with respect to the cell temperature to change the relative humidity (R.H.). The cell temperature was measured by a thermocouple embedded in the cathodic graphite plate, close to the MEA.

Steady-state galvanostatic polarization experiments in PEMFC were performed in the presence of H_2–O_2 at various temperature, R.H. and pressure conditions. Electrochemical data were not corrected for gas cross-over. Cyclic voltammetry (CV) studies were carried out at 80 °C. In this experiment, hydrogen was fed to the anode that operated as both counter and reference electrode, whereas, nitrogen was fed to the working electrode. The sweep rate was 0.15 V s^{-1}. Accelerated degradation tests in PEMFC consisted of 10^4 step cycles between cell voltages of 0.6 V and 0.9 V in the presence of H_2 feed at the anode and O_2 feed at the cathode. This accelerated test was made under automotive relevant temperature and R.H. conditions (110 °C, 33% R.H.). After the electrochemical degradation test, the cathode layer was detached from the membrane and ex-situ characterized by physico-chemical analyses to evaluate sintering and dissolution phenomena.

3. Results and discussion

3.1. Catalyst structure and morphology

X-ray fluorescence analysis confirmed the nominal metal content in both 5%Pt–Pd_3Co_1 catalysts (Table 1); thermal gravimetry analysis indicated a similar total metal concentration (50 ± 2 wt.%). XRD patterns of the carbon-supported 5%Pt–Pd_3Co_1 catalysts are reported in Fig. 1. The catalysts showed a disordered face centered cubic structure (fcc) for both samples. Line broadening analysis of the 220 reflection (Fig. 1) indicated a crystallite size of about 6.2 and 4.4 nm for the two-step and one-step prepared catalysts, respectively. The diffraction pattern of a 50% Pt_3Co_1/C catalyst with similar crystalline structure is also shown for comparison. The mean crystallite size for the latter catalyst was about 3 nm.

TEM analysis (Fig. 2a) showed a good dispersion for the composite Pd-based catalyst subjected to a one-step reduction. Whereas the catalyst prepared by the two-step procedure showed some agglomeration (Fig. 2b). The mean particle size from TEM was essentially similar to the crystallite size determined by XRD in both samples confirming the particle growth in the two-step sample. As comparison, the 50% Pt_3Co_1/C sample showed fine and well dispersed particles (Fig. 2c).

3.2. Electrochemical studies at conventional temperature

The electrochemically active surface area (ECSA) of the Pt–PdCo catalysts has been investigated in-situ at 80 °C by using cyclic voltammetry (Fig. 3). Generally, the hydrogen adsorption region

Table 1
Physico-chemical properties of the catalysts.

Sample	Crystallite size XRD, nm	Pt:Pd:Co XRF bulk atomic content, %	Pt:Pd:Co XPS near surface atomic content, %	Pt:Pd:Co LE-ISS outermost layer atomic content, %
5%Pt–Pd_3Co_1/C one-step	4.4	2.8:72.7:24.5	8.13:72.44:19.43	7.2:80.3:12.5
5%Pt–Pd_3Co_1 two-steps	6.2	2.6:73.1:24.3	15.42:79.43:5.14	15.6:80.6:3.8
Pt_3Co_1	2.9	77.3:22.7	–	-

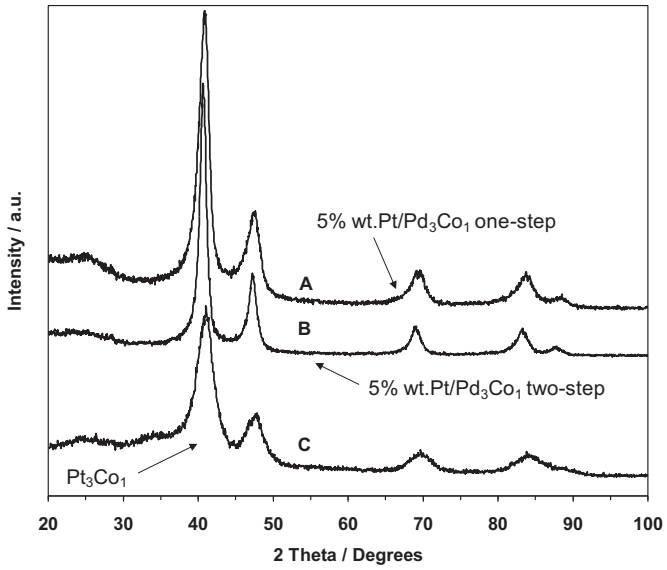

Fig. 1. XRD patterns of carbon-supported 5% wt. Pt–95% wt. Pd_3Co_1 electrocatalysts prepared by the one-step (A) and two-step (B) processes. The XRD pattern of carbon-supported Pt_3Co_1 (C) is reported for comparison.

(0.05–0.4 V RHE) is used to determine the electrochemical active surface area (ECSA) of Pt catalysts. In the case of Pd-based catalysts, this procedure should be used with caution since the stoichiometry of hydrogen adsorbed on Pd is not known exactly as in the case of Pt; however, such approach offers a basis to compare the ECSA for the various catalysts. The ECSA of the PtCo alloy used for comparison was 55 $m\,g^{-1}$ [42]. The value determined for the two-step Pd-based catalyst was about 41 $m\,g^{-1}$ compared to 26 $m\,g^{-1}$ for the one-step catalyst. The ECSA results obtained for the Pd-based catalyst are opposite to what envisaged from the particle size and morphology characteristics (XRD, TEM). Probably, other aspects such as catalyst surface chemistry or electronic properties play a more relevant role than the morphology. The Pd-based catalysts show different profiles in the hydrogen desorption–adsorption region and in the region of OH adsorption. The peak associated with strongly adsorbed hydrogen appears more evident in the two-step catalyst whereas the peak related to the desorption of weakly adsorbed hydrogen is more relevant in the one-step catalyst. There is a larger convolution in the H-desorption peaks in the two-step catalyst; this feature reveals a stronger degree of interaction between Pd and Pt. Similarly, OH adsorption at high potentials firstly occurs for the two-step catalyst (0.65 V RHE). This is not always considered as a positive effect; however, DFT studies have shown that a direct correlation between the coverage of oxygenated species on the electrocatalyst surface and the intrinsic catalytic activity is not straightforward [47]. Moreover, the oxide reduction peak occurs at a similar potential for both catalysts (0.75 V RHE). Thus, the different onset for OH adsorption may be just due to a different voltammetric profile in the double layer region.

The electrocatalytic activity towards the oxygen reduction reaction has been in-situ investigated in a PEMFC single cell at different temperatures (80–130 °C). The membrane used in these experiments was Nafion 115. Since Nafion-type membranes easily dehydrate above 90 °C, it was necessary to raise the pressure up to 3 bars abs to retain a fraction of liquid water inside the MEA.

The PEMFC polarization curves carried out at 80 °C and full humidification (Fig. 4a) showed significantly better performance for the Pt–PdCo catalyst obtained by the two-step procedure confirming the indication provided by CV analysis in terms of

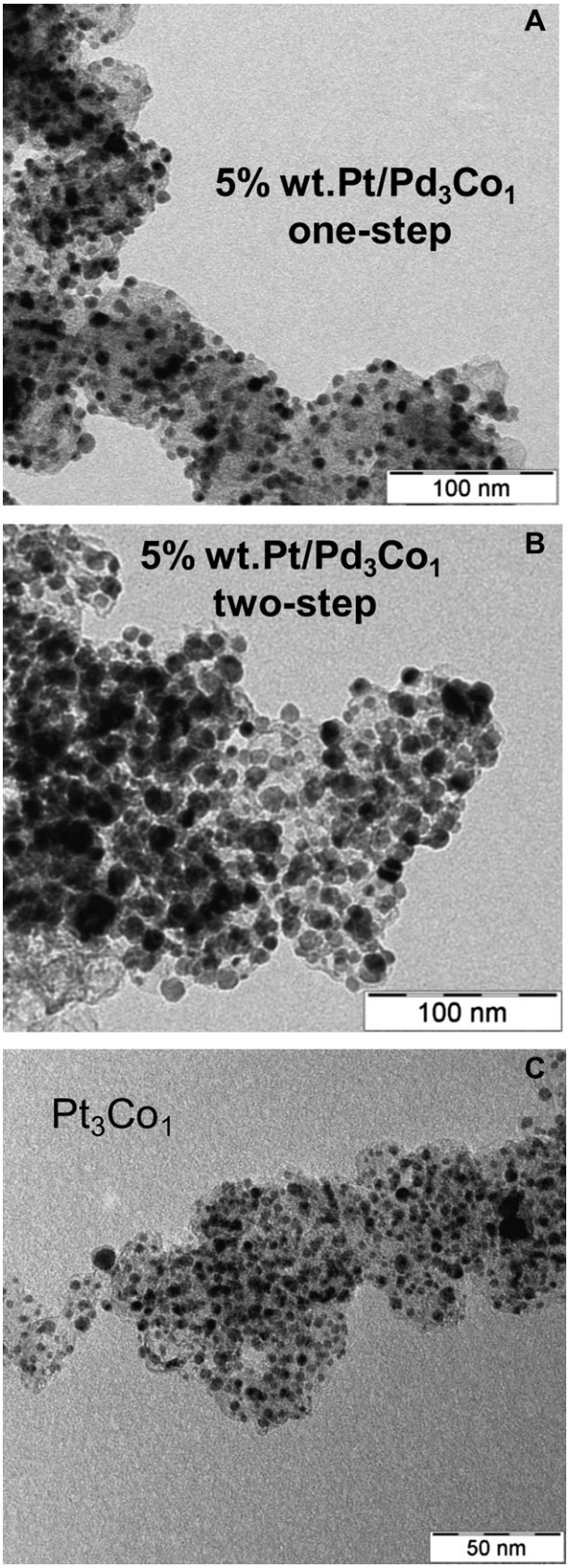

Fig. 2. Transmission electron micrographs of carbon-supported 5% wt. Pt–95% wt. Pd_3Co_1 electrocatalysts prepared by the one-step (A) and two-step (B) processes. The micrograph of carbon-supported Pt_3Co_1 (C) is reported for comparison.

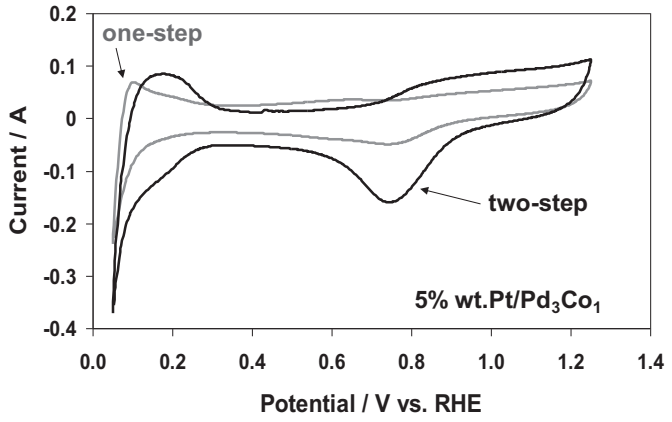

Fig. 3. In-situ cyclic voltammetry analysis of carbon-supported 5% wt. Pt–95% wt. Pd_3Co_1 electrocatalysts prepared by the one-step (gray-line) and two-step (black-line) processes.

electrochemically active surface area. However, under conventional operating conditions, the performance of the best Pt–PdCo catalyst did not reach that of a Pt_3Co_1 alloy with same crystallographic structure (fcc) and smaller (~3 nm) particle size [42]. It should be pointed out that the Pt_3Co_1 alloy electrode contained a slightly larger noble metal loading (0.3 mg cm^{-2}) than the Pt–PdCo catalysts (0.255 mg cm^{-2}); however, this did not justify the significantly different performance at 80 °C and full humidification. It clearly appears that the oxygen reduction rate at 80 °C with full humidification is definitively better for the Pt-alloy catalyst. However, it is important to stress that the Pt–PdCo catalyst has a Pt content of only 15 μg cm^{-2} compared to 300 μg cm^{-2} in the Pt_3Co_1 alloy electrode. Ohmic-drop corrected Tafel curves with the current normalised with respect the total noble metal loading are reported in Fig. 4b. These curves provide an indication of the electrocatalytic activity in the activation controlled region. The Tafel plots clearly showed better electrocatalytic activity for the Pd catalyst prepared by the two-step process with respect to the one-step catalyst but lower activity than the Pt-alloy. The Tafel slope of about 70 mV/dec registered for the Pd-based catalysts was similar to that observed for the PtCo catalyst. This is the value expected for a Temkin isotherm adsorption condition for the coverage of oxygenated species [48]. The mass activity registered at 0.9 V for the best Pt–PdCo was about 65 mA/mg$_{Pd+Pt}$ at 80 °C (Table 2); but if normalised by the Pt content only (as it would be appropriate from a practical point of view being the cost of Pt much higher than Pd), it increases to more than 1100 mA/mg$_{Pt}$. A value that is much higher than those obtained with benchmark Pt-alloy catalysts measured under fuel cell operation. The mass activity of the PtCo used for comparison was about 360 mA/mg. Of course, Pd does not act simply as a spectator during the oxygen reduction process or it is just a simple core support for Pt since it effectively contributes to the oxygen reduction reaction [35,49].

If one considers that the ECSA of the two-step Pt–PdCo catalyst is lower than that of the carbon-supported PtCo alloy, part of the gap between the overall mass activities of these catalysts may arise from the different catalyst utilization. Whereas, it is less clear why the one-step preparation procedure, allowing to obtain Pd-based catalyst with particle size comparable to that of Pt-based catalyst, gives rise to a poorly performing catalyst.

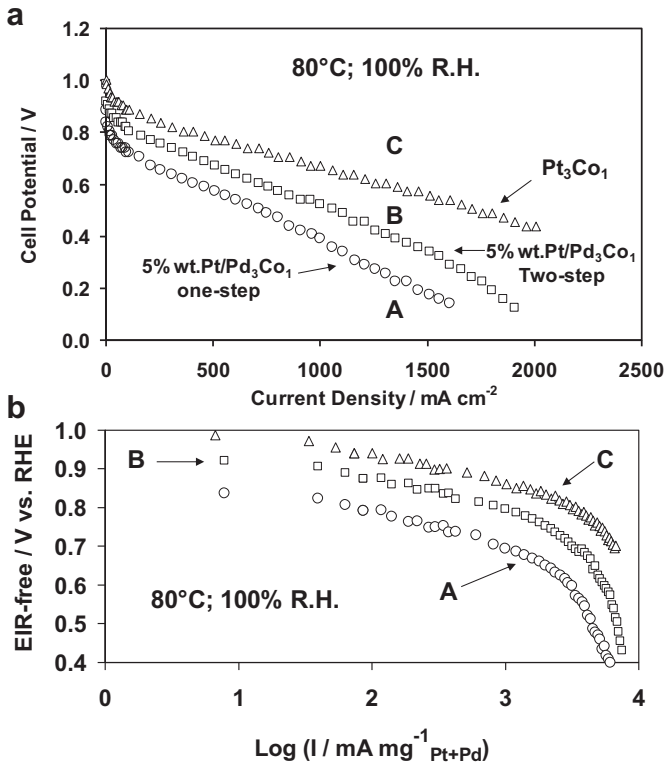

Fig. 4. Polarization curves (a) and corresponding Tafel plots (b) of the carbon-supported 5% wt. Pt–95% wt. Pd_3Co_1 electrocatalysts prepared by the one-step (A) and two-step (B) processes at 80 °C and 100% R.H., 3 bar abs.; the carbon-supported Pt_3Co_1 catalyst (C) is reported for comparison. Catalyst loadings: Pt 0.015 mg cm^{-2}, Pd 0.24 mg cm^{-2} in the Pd-based electrodes; Pt 0.3 mg cm^{-2} in the Pt_3Co_1 alloy electrode.

3.3. Surface characteristics

To get more insights into these aspects and to better understand why Pd-based catalysts prepared in different ways give rise to a quite different CV profile, we have investigated the surface chemistry by using two complementary techniques (XPS and LE-ISS). A typical XPS study involves an analysis depth of 2–3 nm (near surface region) inside the sample. Direct information about the top-most atomic layer is provided by LE-ISS. However, the latter technique does not give any information about the electronic levels. A combination of both techniques can provide a more complete picture [42].

The survey XP-spectra are shown in Fig. 5. The relative atomic concentrations of Pt, Pd and Co are reported in Table 2. Both Pd catalysts preparation procedures give rise to an enrichment of Pt on the surface. It is also observed that the Co concentration in the near surface region is much smaller for the two-step catalyst; moreover, this sample shows a significantly larger Pt/Pd ratio compared to the one-step catalyst. The Pt enrichment on the surface of the catalyst prepared by the two-step method appears to be due to a preferential interaction of Pt with the already formed PdCo particles instead than with carbon support. Another important aspect is, however, related to the surface oxidation states. The high-resolution spectra of the Pd 3d and Pt 4f photoelectron peaks

Table 2
Mass activity for oxygen electroreduction under conventional and automotive aimed conditions.

Operating conditions	5%Pt–Pd_3Co_1 two-steps mass activity at 0.9 V RHE, mA/mg$_{Pt+Pd}$	Pt_3Co_1 mass activity at 0.9 V RHE, mA/mg$_{Pt+Pd}$
80 °C; 100% R.H.	65	360
110 °C; 33% R.H.	120	185

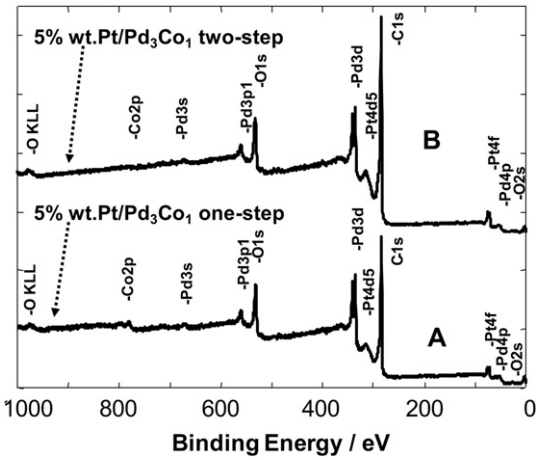

Fig. 5. Survey X-ray photoelectron spectra of the carbon-supported 5% wt. Pt–95% wt. Pd_3Co_1 electrocatalysts prepared by the one-step (A) and two-step (B) processes.

(Fig. 6a and b) reveal that the Pd is in a metallic form in both catalysts whereas a significant fraction of surface sites characterised by a Pt^{2+} state is observed in the catalyst obtained by the one-step process (e.g. $Pt(OH)_2$). This effect is due to a strong interaction of Pt with the carbon black functional groups [50,51] in the one-step catalyst. Such interaction probably favours the dispersion and thus the occurrence of finer particles. Yet, a significant presence of oxidised surface sites may hinder the adsorption of oxygen molecules during the ORR. The analysis of the top-most surface atomic layer by LE-ISS (Fig. 7, Table 1) shows a low Co content and a significant enrichment in Pt in the two-step process. It is assumed that Pt nucleation on pre-formed metallic Pd-based particles may give rise easily to metallic Pt sites; whereas interaction with oxygenated functional groups of the carbon support may favour surface oxidation. However, Pt sites cover only in part the Pd core particles even in the two-step catalyst since LE-ISS spectra show significant Pd content in the outermost layer (Fig. 7). In our opinion the three main characteristics of the composite Pd catalyst obtained by the two-step method (Pt enrichment in the outermost layer, small Co content on the surface, surface Pt sites in a metallic state) determine its significantly better performance than the one-step catalyst. Moreover, since larger particle size and lower particle dispersion characteristics have been observed by TEM for the two-step catalyst vs. the one-step sample, it is derived that the surface chemistry and the electronic levels play a role more relevant than the morphology in these materials.

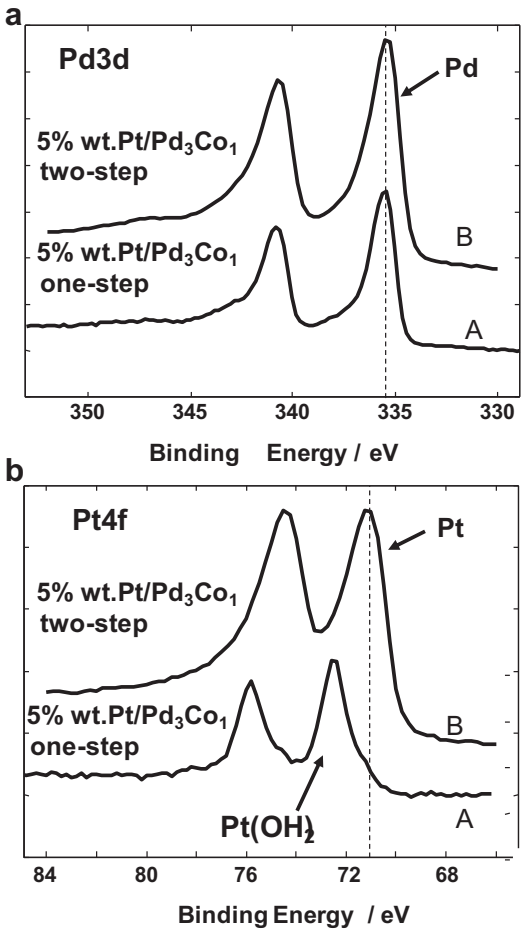

Fig. 6. High-resolution X-ray photoelectron spectra of the carbon-supported 5% wt. Pt–95% wt. Pd_3Co_1 electrocatalysts prepared by the one-step (A) and two-step (B) processes. (a) Pd 3d; and (b) Pt 4f.

3.4. Electrochemical studies at intermediate temperatures

It is a common opinion that the future fuel cell based electric vehicle may operate in a temperature range of 110–130 °C as well as at low relative humidity (<33%) to reduce thermal and water management constraints [52].

Fig. 8a shows the effect of temperature on the polarization curves obtained under full humidification for the two-step Pd catalyst. It is observed that the performance increases up to 110 °C whereas it decreases significantly at 130 °C. Generally, MEAs based on Pt catalysts and PFSA membranes show a performance decrease above 80 °C especially due to the ionomer and membrane dry-out. This effect is reduced in the presence of a suitable pressure, e.g. 3 bar abs. At relevant pressure there is a small amount of liquid water present inside the MEA but the negative effect caused by dehydration is, however, present [7]. The results here observed for the Pd-based catalyst instead indicate that its performance is activated by the temperature at least up to 110 °C whereas the negative effect of dehydration becomes relevant at higher temperature.

When the relative humidity is decreased to 33%, no relevant differences are seen in the temperature range from 80 to 110 °C for

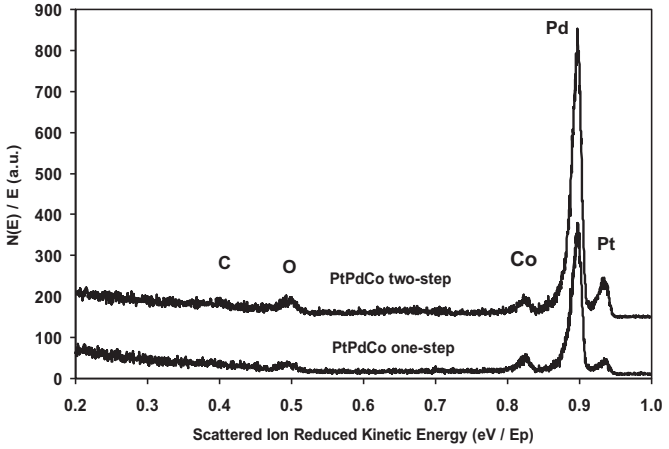

Fig. 7. Low-energy ion scattering spectroscopy ($3He^+$, 1 kV) of carbon-supported 5% wt. Pt–95% wt. Pd_3Co_1 electrocatalysts prepared by the one-step (A) and two-step (B) processes.

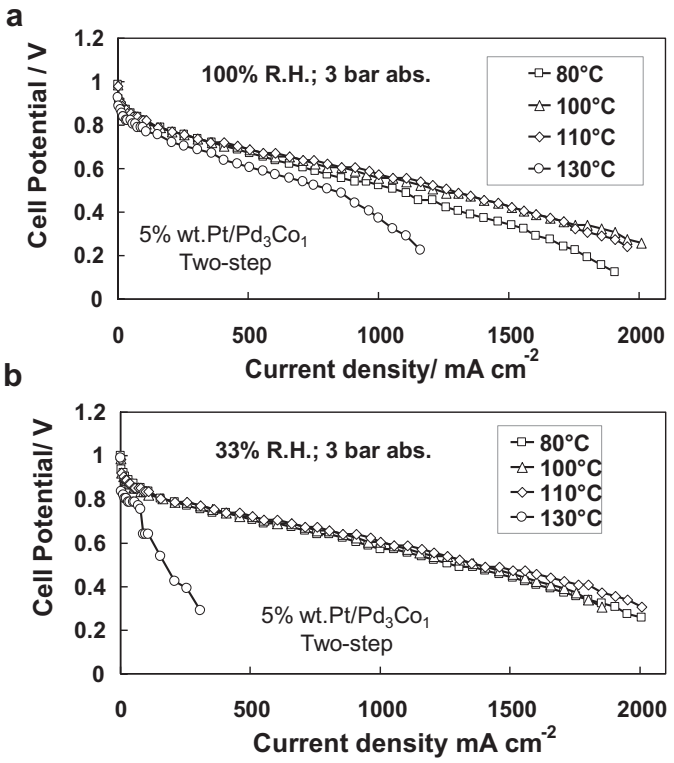

Fig. 8. Effect of the temperature on the polarization behaviour for the carbon-supported 5% wt. Pt–95% wt. Pd_3Co_1 electrocatalysts prepared by the two-step processes at 3 bar abs. (a) 100% R.H.; (b) 33% R.H. Catalyst loading: Pt 0.015 mg cm^{-2} and Pd 0.24 mg cm^{-2}.

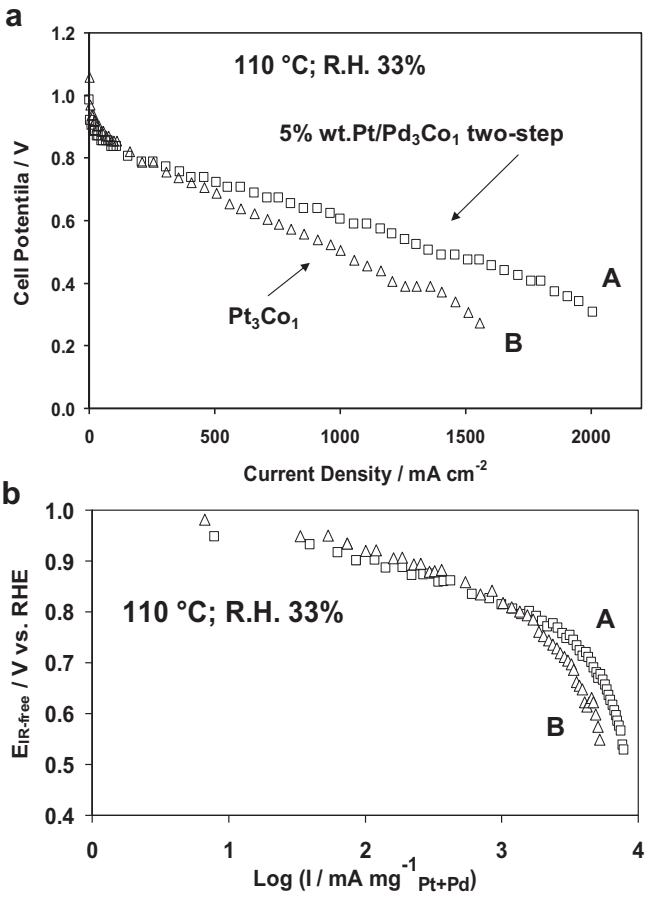

Fig. 9. Comparison of the polarization behaviour (a) and Tafel plots (b) for the carbon-supported 5% wt. Pt–95% wt. Pd_3Co_1 (A) and the Pt_3Co_1 (B) electrocatalysts at 110 °C and 33% RH. Catalyst loadings: Pt 0.015 mg cm^{-2}, Pd 0.24 mg cm^{-2} in the Pd-based electrode; Pt 0.3 mg cm^{-2} in the Pt_3Co_1 alloy electrode.

the two-step Pd-based catalyst (Fig. 8b). Under these conditions, dehydration effects are more critical and thus compensate the temperature activation effect previously observed under full humidification. However, the performance recorded under 33% R.H. is not significantly lower than that recorded with 100% R.H. (Fig. 8). This indicates that for the Pd-based catalyst there is a strong temperature activation and it compensates, for the effect of dehydration up to 110 °C under the present conditions. The ohmic drop does not increase significantly with the temperature up to 110 °C since the pressure allows to maintain a suitable fraction of liquid water as necessary to assure good conductivity within the membrane. However, water is also essentially to transport protons within the catalytic layer. Under these conditions (110 °C), the main effect of decreasing R.H. concerns with ionomer dry-out. Different is the case of 130 °C and R.H. 33% operating conditions where the effects of high temperature and low R.H. cause both ionomer dry-out and an increase of the ohmic resistance for the membrane.

Quite interesting is the comparison of performance at 110 C and low R.H. 33% (a condition suitable for automotive applications) for the two-step Pd-based catalyst and the Pt_3Co_1 alloy characterised by the same crystallographic structure and smaller particle size (Fig. 9). At low current density, where the activation control is prevailing, it appears that most of the performance gap between the Pd-based catalyst and the Pt_3Co_1 alloy previously observed at 80 °C and full humidification is recovered at 110 °C and 33% R.H. (Fig. 9). The Tafel plots (Fig. 9b) indicate that in the activation controlled region the Pt_3Co_1 alloy is still characterised by slightly better mass activity; however, at high current densities the Pd-composite catalyst is better performing. The latter aspect is likely not related to the intrinsic catalytic activity but to morphology aspects since at high currents mass transport characteristics are prevailing. We interpret this effect as due to the fact that being the Pd-based catalyst characterised by larger particles, the catalytic sites are more accessible under conditions where ionomer dehydration limits the extension of the catalyst-electrolyte interface to the outer catalyst pores only. We have made some attempts to increase slightly the particle size of the PtCo alloy catalyst by increasing the temperature of the carbothermal reduction to verify this hypothesis but it was correspondingly observed a change in the crystallographic structure from disordered face centered cubic to a primitive cubic ordered ($L1_2$) phase making such a comparison meaningless. We have indeed observed an increase of performance at intermediate temperature and at high current densities for the PtCo alloy catalyst with primitive cubic structure and slightly larger particle size than the present one as reported in an earlier paper [53].

The Tafel slope was around 85 mV at 110 °C for both Pd-based and PtCo catalysts (Fig. 9b). This increase in the Tafel slope is not associated to a change in the oxygen adsorption properties or the mechanism but it is simply due to the increase of temperature.

A suitable performance under automotive relevant conditions is however not sufficient to assess the perspectives of utilization of such Pd-based electrocatalyst. It is also important to verify that a suitable performance is associated to a good stability [34]. We have thus carried out an accelerated degradation test (ADT) consisting of 10^4 electrochemical step cycles between 0.6 and 0.9 V at 110 °C and 33% R.H. [42]. Afterwards, polarization curves were

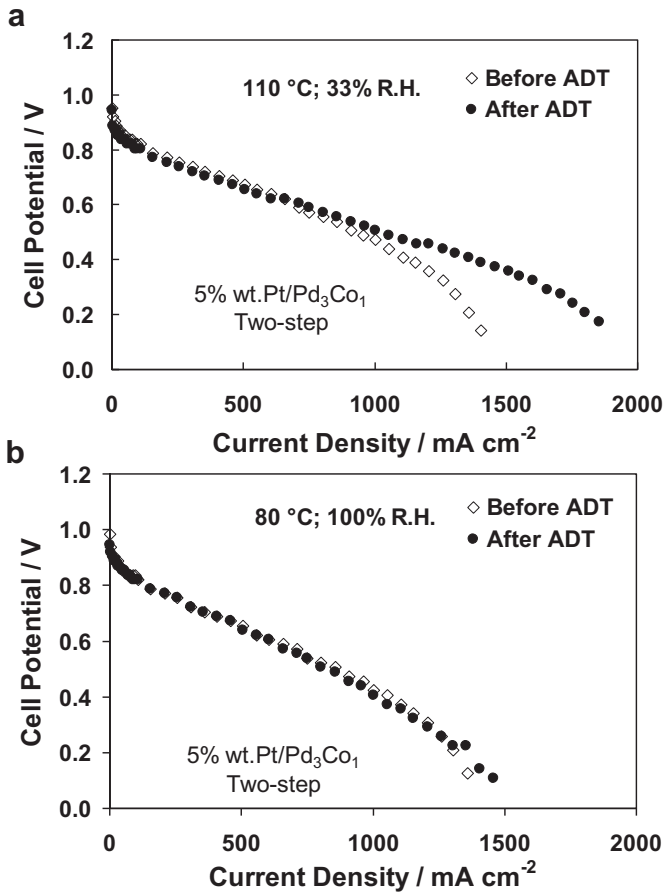

Fig. 10. Polarization curves before and after the accelerated degradation test (potential cycling 0.6–0.9 V at 110 °C, 33% R.H.) for the two-step carbon-supported 5% wt. Pt–95% wt. Pd_3Co_1 electrocatalyst: (a) 110 °C and 33% RH; (b) 80 °C and 100% R.H. Catalyst loading: Pt 0.012 mg cm^{-2} and Pd 0.19 mg cm^{-2}.

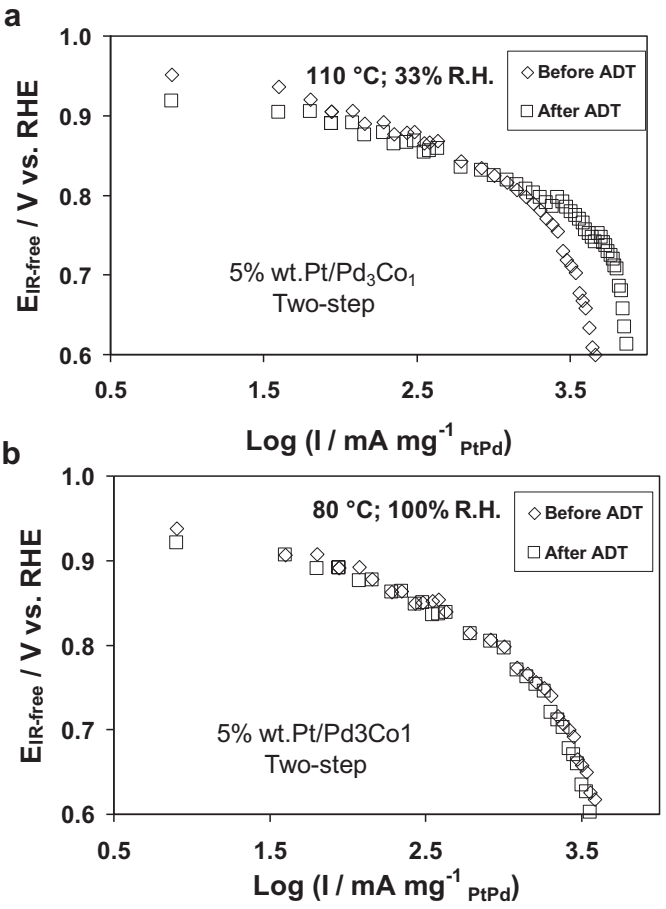

Fig. 11. Tafel plots before and after the accelerated degradation test (potential cycling 0.6–0.9 V at 110 °C, 33% R.H.) for the two-step carbon-supported 5% wt. Pt–95% wt. Pd_3Co_1 electrocatalyst: (a) 110 °C and 33% R.H.; (b) 80 °C and 100% R.H. Catalyst loading: Pt 0.012 mg cm^{-2} and Pd 0.19 mg cm^{-2}.

recorded both under these conditions (110 °C and 33% R.H.) and at 80 °C, full humidification (Fig. 10a and b). The MEA used for this test contained a lower catalyst loading with respect to those used in performance tests.

After the degradation test, it is just observed a slight decrease of performance in the activation controlled region that appears somewhat more evident in the Tafel plots (Fig. 11a and b). On the contrary, an increase of limiting current was registered after the ADT at 110 °C. This reveals a decrease of mass transport constraints corresponding to a reduction of voltage losses at high current density after cycled operation (Fig. 11). The latter phenomenon may be associated to a change in the catalytic layer flooding characteristics at high temperature and high current densities. However, in the range of technical interest, i.e. at intermediate voltages the performance is similar before and after the accelerated test. The comparison of cyclic voltammetry profiles (Fig. 12) before and after the degradation test indeed shows a decrease of the electrochemically active surface area but also a shift of the PdO and/or PtO reduction peak to higher potentials corresponding to an increase of intrinsic catalytic activity [7]. These effects possibly compensate each other. Indeed the comparison of the catalytic layer diffraction pattern obtained after cycled operation and the pattern of the raw catalyst powder do not reveal significant change in peak broadening for the 220 reflection (Fig. 13). This peak is the one less affected by the presence of ionomer and backing layer. The new peak observed at 25° two-theta is due to the presence of carbon fibres from carbon cloth backing and specifically to the (002) reflection of the graphite hexagonal structure. Probably, the loss of surface area is not due to an increase of the mean crystallite size but to some agglomeration with consequent loss of dispersion as can be envisaged from the TEM micrograph of the catalytic layer after cycled operation (Fig. 14).

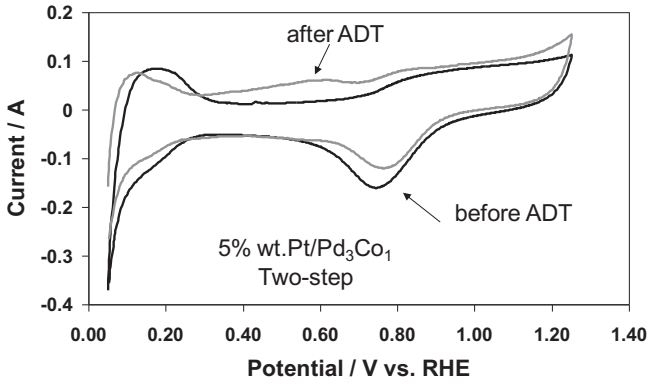

Fig. 12. Cyclic voltammograms of the two-step carbon-supported 5% wt. Pt–95% wt. Pd_3Co_1 electrocatalyst before (catalyst powder) and after (catalytic layer) the accelerated degradation test.

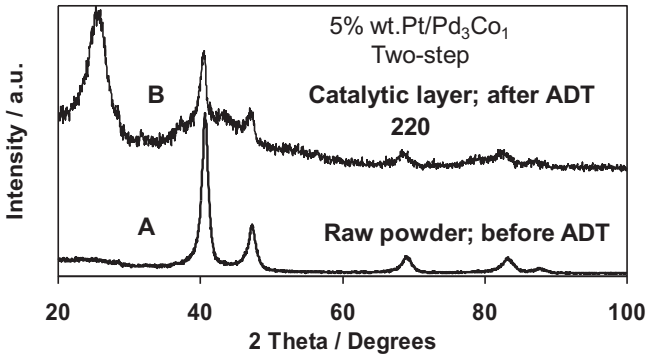

Fig. 13. X-ray diffraction patterns of the two-step carbon-supported 5% wt. Pt–95% wt. Pd_3Co_1 electrocatalyst before (catalyst powder) and after (catalytic layer) the accelerated degradation test.

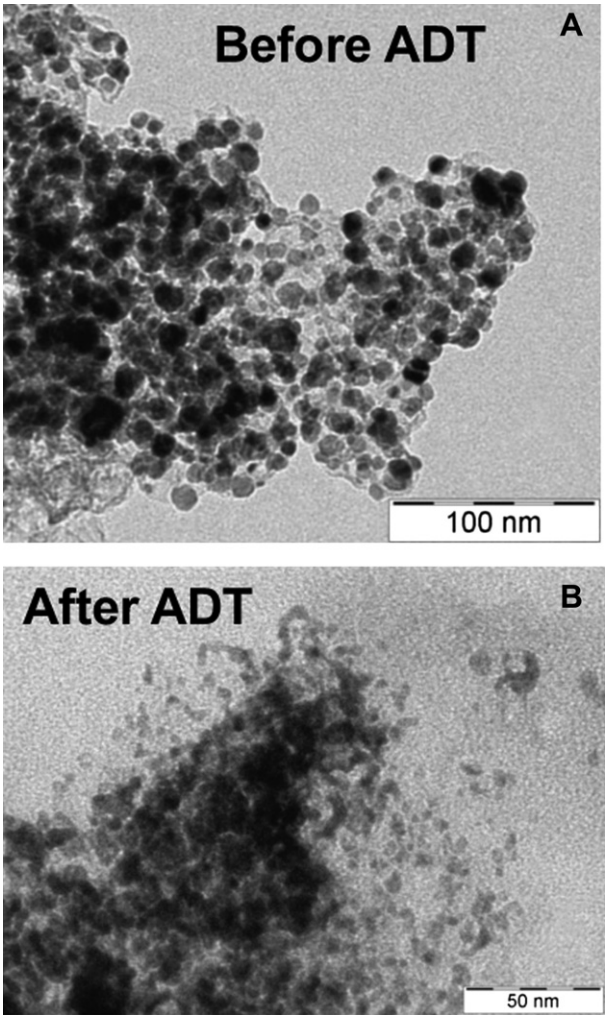

Fig. 14. Transmission electron micrographs of the two-step carbon-supported 5% wt. Pt–95% wt. Pd_3Co_1 electrocatalyst before and after the accelerated degradation test.

4. Conclusion

Composite 5%Pt–Pd_3Co_1 catalyst obtained from the two preparation routes were investigated for the oxygen reduction process in PEMFCs. It was observed that formation of a core Pd_3Co_1 alloy followed by deposition of a Pt overlayer with two different reduction steps produced an enrichment of Pt in the outermost layers and a lower degree of interaction with carbon functional groups. This gave rise to an increase of the electrochemically active surface area despite a larger particle size with respect to a Pd-based catalyst prepared in a single step. The electrocatalytic activity of the two-step Pd-based catalyst increased considerably by increasing the temperature from 80 to 110 °C at low relative humidity (R.H. 33%). Whereas, an opposite effect was observed for a conventional PtCo alloy catalyst with similar crystallographic structure but characterised by finer particles. It appears that the strong temperature activation for the Pd-based catalyst at low current densities where catalytic effects are important and compensates the negative effect of ionomer dry-out at intermediate temperatures that is instead prevailing for the PtCo catalyst. At high current densities where mass transport phenomena are relevant, catalyst morphology probably influences the performance at intermediate temperatures and low R.H. operating conditions in a manner different than at conventional operating conditions (80 °C, high R.H.). However, a systematic investigation of catalysts with different morphologies but with the same structural and surface characteristics is necessary to confirm this conjecture.

Acknowledgements

The authors acknowledge the financial support of the EU through the QuasiDry Project 256821. “The research leading to these results has received funding from the European Community’s Seventh Framework Programme (FP7/2010–2013) under the call ENERGY-2010-10.2-1: Future Emerging Technologies for Energy Applications (FET).”

Special thanks are due to Mr. G. Monforte for XPS and LE-ISS measurements.

References

[1] A.S. Aricò, P. Bruce, B. Scrosati, J.-M. Tarascon, W. Van Schalkwijk, Nat. Mater. 4 (2005) 366–377.
[2] H.A. Gasteiger, S.S. Kocha, B. Sompalli, F.T. Wagner, Appl. Catal. B: Environ 56 (2005) 9–35.
[3] R.L. Borup, J.R. Davey, F.H. Garzon, D.L. Wood, M.A. Inbody, J. Power Sources 163 (2006) 76–81.
[4] H.R. Colon-Mercado, B.N. Popov, J. Power Sources 155 (2006) 253–263.
[5] K. Jayasayee, T.D. Van Anh, T. Verhoeven, S. Celebi, F.A. De Bruijn, J. Phys. Chem. C 113 (2009) 20371–20380.
[6] P. Strasser, S. Koh, T. Anniyev, J. Greeley, K. More, C. Yu, Z. Liu, S. Kaya, D. Nordlund, H. Ogasawara, M.F. Toney, A. Nilsson, Nat. Chem. 2 (2010) 454–460.
[7] A.S. Aricò, A. Stassi, E. Modica, R. Ornelas, I. Gatto, E. Passalacqua, V. Antonucci, J. Power Sources 178 (2008) 525–536.
[8] A.S. Aricò, V. Baglio, V. Antonucci, in: Nanotechnology for the Energy Challenge, Wiley-VCH, Weinheim, 2009, pp. 79–109.
[9] M.K. Debe, A.K. Schmoeckel, G.D. Vernstrom, R. Atanasoski, J. Power Sources 161 (2006) 1002–1011.
[10] T.E. Wood, Z. Tan, A.K. Schmoeckel, D. O’Neill, R. Atanasoski, J. Power Sources 178 (2008) 510–516.
[11] G.G. Wildgoose, C.E. Banks, R.G. Compton, Small 2 (2006) 182–193.
[12] V. Stamenkovic, B.S. Mun, K.J.J. Mayrhofer, P.N. Ross, N.M. Markovic, J. Rossmeisl, J. Greeley, J.K. Norskov, Angew. Chem., Int. Ed. 45 (2006) 2897–2901.
[13] S. Chen, W. Sheng, N. Yabuuchi, P.J. Ferreira, L.F. Allard, Y. Shao-Horn, J. Phys. Chem. C 113 (2009) 1109–1125.
[14] F. Charreteur, F. Jaouen, J.P. Dodelet, Electrochim. Acta 54 (2009) 6622–6630.
[15] W. Chen, J. Akhigbe, C. Bruckner, C.M. Li, Y.J. Lei, Phys. Chem. C 114 (2010) 8633–8638.
[16] R. Bashyam, P. Zelenay, Nature 443 (2006) 63–66.
[17] Y.J. Feng, T. He, N. Alonso-Vante, Chem. Mater. 20 (2008) 26–28.
[18] E. Antolini, S.C. Zignani, S.F. Santos, E.R. Gonzalez, Electrochim. Acta 56 (2011) 2299–2305.
[19] M. Maximov, O.A. Petrii, Elektrokhimiya 10 (1974) 1721–1724.
[20] V. Raghuveer, P.J. Ferreira, A. Manthiram, Electrochem. Commun. 8 (2006) 807–814.
[21] W. Wang, D. Zheng, C. Du, Z. Zou, X. Zhang, B. Xia, H. Yang, D.L. Akins, J. Power Sources 167 (2007) 243–249.

[22] J.J. Salvador-Pascual, S. Citalán-Cigarroa, O.J. Solorza-Feria, Power Sources 172 (2007) 229–234.
[23] M.S. Rau, P.M. Quaino, M.R.G. de Chialvo, A.C. Chialvo, Electrochem. Commun. 10 (2008) 208–212.
[24] A.C. Garcia, V.A. Paganin, E.A. Ticianelli, Electrochim. Acta 53 (2008) 4309–4315.
[25] Y.-H. Cho, B. Choi, Y.-H. Cho, H.-S. Park, Y.-E. Sung, Electrochem. Commun. 9 (2007) 378–381.
[26] J. Zhang, Y. Mo, M.B. Vukmirovic, R. Klie, K. Sasaki, R.R. Adzic, J. Phys. Chem. B 108 (2004) 10955–10964.
[27] J.L. Zhang, M.B. Vukmirovic, Y. Xu, M. Mavrikakis, R.R. Adzic, Angew. Chem., Int. Ed. 44 (2005) 2132–2135.
[28] W.P. Zhou, X. Yang, M.B. Vukmirovic, B.E. Koel, J. Jiao, G. Peng, M. Mavrikakis, R.R. Adzic, J. Am. Chem. Soc. 131 (2009) 12755–12762.
[29] T. Cochell, A. Manthiram, Langmuir 28 (2012) 1579–1587.
[30] H. Li, G. Sun, N. Li, S. Sun, D. Su, Q. Xin, J. Phys. Chem. C 111 (2007) 5605–5617.
[31] S.A. Grigoriev, E.K. Lyutikova, S. Martemianov, V.N. Fateev, Int. J. Hydrogen Energy 32 (2007) 4438–4442.
[32] Z. Liu, L. Hong, M.P. Tham, T.H. Lim, H. Jiang, J. Power Sources 161 (2006) 831–835.
[33] W. Wang, Q. Huang, J. Liu, Z. Zou, Z. Li, H. Yang, Electrochem. Commun. 10 (2008) 1396–1399.
[34] J. Zhao, K. Jarvis, P. Ferreira, A. Manthiram, J. Power Sources 196 (2011) 4515–4523.
[35] Y. Tang, H. Zhang, H. Zhong, T. Xu, H. Jin, J. Power Sources 196 (2011) 3523–3529.
[36] J. Zhao, A. Manthiram, Appl. Catal. B: Environ. 101 (2011) 660–668.
[37] B. Fıçıcılara, A. Bayrakçekenb, İ Eroğlu, J. Power Sources 193 (2009) 17–23.
[38] K.D. Beard, J.W. Van Zee, J.R. Monnier, Appl. Catal. B: Environ. 88 (2009) 185–193.
[39] Z.-M. Zhou, Z.-G. Shao, X.-P. Qin, X.-G. Chen, Z.-D. Wei, B.-L. Yi, Int. J. Hydrogen Energy 35 (2010) 1719–1726.
[40] B. Lim, M. Jiang, P.H.C. Camargo, E.C. Cho, J. Tao, X. Lu, Y. Zhu, Y. Xia, Science 324 (2009) 1302–1305.
[41] M. Shao, K. Shoemaker, A. Peles, K. Kaneko, L. Protsailo, J. Am. Chem. Soc. 132 (2010) 9253–9255.
[42] A.S. Aricò, A. Stassi, I. Gatto, G. Monforte, E. Passalacqua, V. Antonucci, J. Phys. Chem. C 114 (2010) 15823–15836.
[43] J. Peron, Y. Nedellec, D.J. Jones, J. Rozière, J. Power Sources 185 (2008) 1209–1217.
[44] A. Stassi, I. Gatto, E. Passalacqua, V. Antonucci, A.S. Aricò, L. Merlo, C. Oldani, E. Pagano, J. Power Sources 196 (2011) 8925–8930.
[45] L.J. Bonville, H.R. Kunz, Y. Song, A. Mientek, M. Williams, A. Ching, J.M. Fenton, J. Power Sources 144 (2005) 107–112.
[46] J.F. Moulder, W.F. Stickle, P.E. Sobol, K.D. Bomben, in: Handbook of X-ray Photoelectron Spectroscopy, Physical Electronics, Inc, Eden Prairie, MN, 1995.
[47] J. Rossmeisl, G.S. Karlberg, T. Jaramillo, J.K. Norskov, Faraday Discuss. 140 (2008) 337–347.
[48] A.S. Aricò, V. Antonucci, V. Alderucci, E. Modica, N. Giordano, J. Appl. Electrochem. 23 (1993) 1107–1116.
[49] D.N. Son, K. Takahashi, J. Phys. Chem. C 116 (2012) 6200–6207.
[50] A.S. Aricò, V. Antonucci, M. Minutoli, N. Giordano, Carbon 27 (1989) 337–347.
[51] A.S. Aricò, V. Antonucci, L. Pino, P.L. Antonucci, N. Giordano, Carbon 28 (1990) 599–609.
[52] A.S. Aricò, A. Di Blasi, G. Brunaccini, F. Sergi, G. Dispenza, L. Andaloro, M. Ferraro, V. Antonucci, P. Asher, S. Buche, D. Fongalland, G.A. Hards, J.D.B. Sharman, A. Bayer, G. Heinz, N. Zandonà, R. Zuber, M. Gebert, M. Corasaniti, A. Ghielmi, D.J. Jones, Fuel Cells 10 (2010) 1013–1023.
[53] A. Stassi, I. Gatto, G. Monforte, V. Baglio, E. Passalacqua, V. Antonucci, A.S. Aricò, J. Power Sources 208 (2012) 35–45.